Pure Appl. Geophys. 176 (2019), 4401–4414

https://doi.org/10.1007/s00024-019-02212-5

Pure and Applied Geophysics

Decompensative Gravity Anomalies Reveal the Structure of the Upper Crust of Antarctica

Carina Haeger[1,2] and Mikhail K. Kaban[1,3]

Abstract—As Antarctica is almost entirely covered by thick ice shields impeding in situ measurements, information about upper crustal structures and sedimentary basins is still sparse and the analysis of the gravity anomalies offers new insights. Isostatic gravity anomalies are often used to investigate upper crust structures. However, compensating masses significantly reduce the gravity effect of unknown sedimentary and upper crustal structures. To separate these effects, we apply so-called decompensative corrections to the isostatic anomalies for the Antarctic continent, which reach values of up to ± 70 mGal. The obtained decompensative anomalies well correspond to the known sedimentary basins, such as in the areas of the Filchner-Ronne Ice Shelf and Lambert Graben, and also suggest the existence of other large sedimentary deposits both in West and East Antarctica, which are not or only sparsely mapped by existing seismic surveys, e.g. in coastal Dronning Maud Land and Enderby Land. A dipole-like structure exists at the Transantarctic Mountains and the Wilkes Subglacial Basin, suggesting the presence of isostatic disturbances linked to the dynamic uplift of the Transantarctic Mountains and thick sedimentary accumulations in the east. Extended positive anomalies in East Antarctica are likely related to the old and dense cratonic crust as well as to isostatic disturbances caused by the transition from local to regional compensation around the Lambert Graben.

Key words: Antarctica, decompensative gravity anomaly, upper crust, sediments, gravity modeling.

1. Introduction

In recent years, big efforts have been made to unveil the structure of the Antarctic crust and lithosphere using a variety of geophysical measurements. However, in situ measurements are strongly hindered by the ice shield covering 99% of the continent with thicknesses of up to 4.5 km (Fig. 1b). Hence, knowledge of upper crustal structures and sediment distribution is still limited, especially in central Antarctica. In particular, thickness and properties of sediments also impact ice dynamics by influencing basal controls and likely facilitating the onset of streaming flow (Smith et al. 2013). Therefore, several studies about sediment distribution were conducted below ice streams (e.g., Bamber et al. 2006; Bell et al. 1998). Significant amounts of sediments were also discovered below ice shelfs with up to 8 km in the Ross Ice Shelf (e.g., Trey et al. 1999; Wobbe et al. 2014) or up to 14 km in the Filchner-Ronne Ice Shelf (e.g., Hübscher et al. 1996; Leitchenkov and Kudryavtzev 1997), in the Wilkes Subglacial Basin (up to 7 km, Frederick et al. 2016) and in the Adventure Trench (∼ 10 km, Ferraccioli et al. 2001) using mainly gravity, magnetic and seismic data. Aitken et al. (2014) used gravity signals and depth to magnetic basement to detect several sediment basins within Wilkes Land. Global information about sediment thickness are available from CRUST1.0 (Laske et al. 2013), however, data coverage over Antarctica is sparse. Baranov et al. (2018) compiled existing surveys to create an Antarctica-wide map of sediment thickness but were still faced with large gaps in data in the continental interior that they filled by using a numerical interpolation scheme involving bedrock topography information (Fretwell et al. 2013).

Gravity anomalies have been used successfully before for investigation of density structures of the upper crust in other continents. Commonly, the isostatic anomalies of the gravity field are employed for these purposes since the effect of deep density variations can be effectively reduced from the observed field by applying the isostatic correction (e.g. Simpson et al. 1986; Blakely 1995). The

[1] Deutsches GeoForschungsZentrum Potsdam, Telegrafenberg A20, 14473 Potsdam, Germany. E-mail: carina.haeger@gfz-potsdam.de; kaban@gfz-potsdam.de
[2] Free University Berlin, Berlin, Germany.
[3] Schmidt Institute of Physics of the Earth, Moscow, Russia.

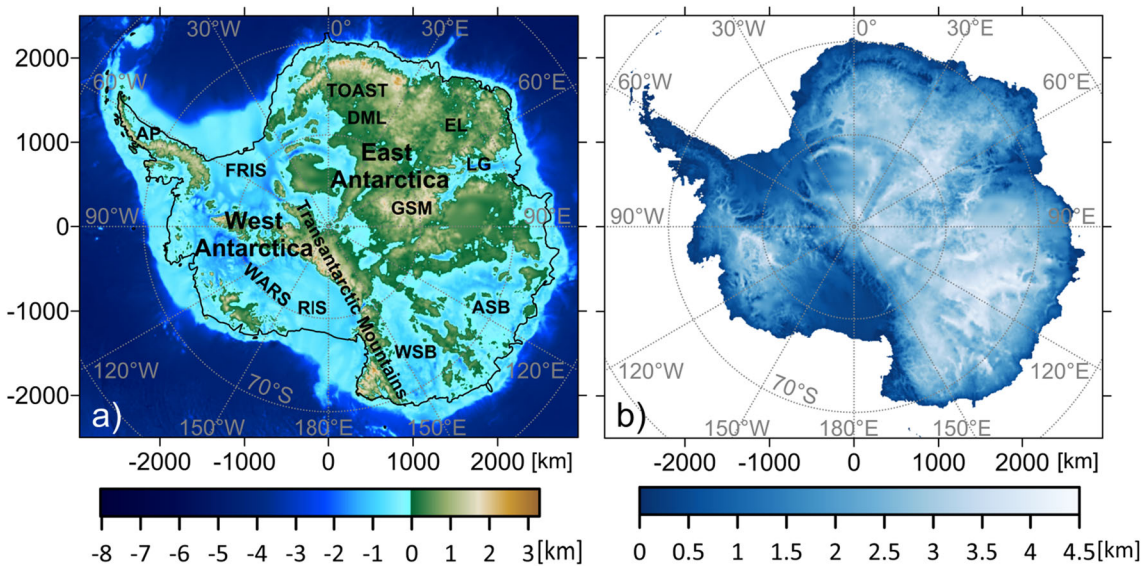

Figure 1

a Bedrock topography of Antarctica (Fretwell et al. 2013) and bathymetry of the surrounding ocean (Schaffer and Timmermann 2016). Key tectonic units: *AP* Antarctic Peninsula, *ASB* Aurora Subglacial Basin, *DML* Dronning Maud Land, *EL* Enderby Land, *FRIS* Filchner-Ronne Ice Shelf, *GSM* Gamburtsev Subglacial Mountains, *LG* Lambert Glacier, *RIS* Ross Ice Shelf, *TOAST* Tonian Oceanic Arc Super Terrane, *WARS* West Antarctic Rift System, *WSB* Wilkes Subglacial Basin and **b** ice thickness (Fretwell et al. 2013)

isostatic anomalies are computed by subtracting the effect of the deep density variations from the Bouguer gravity anomalies, i.e. associated with Moho undulations that balance the topography load according to an expected isostatic compensation model (e.g. Simpson et al. 1986). If the principal parameters of the compensating scheme, chiefly the depth of the compensation and the effective elastic thickness of the lithosphere, are chosen correctly, the local and mid-wave components of the residual isostatic anomalies should reflect the density structure of the upper crust. The long-wavelength anomalies, which reflect the effects of the mantle convection and glacial-isostatic adjustment, can be easily filtered out from the residual field (Kaban et al. 2004). The isostatic anomalies were often used for investigations of sedimentary basins all over the World, e.g. in Nevada (Jachens and Moring 1990), the Los Angeles Basin (Langenheim and Jachens 1996) and Barents Sea (Ebbing et al. 2007). In Antarctica, the isostatic gravity anomalies constrained with other geophysical data sets such as aeromagnetic measurements have been analysed to infer thickness of sediments across the Wilkes Subglacial Basin (Frederick et al. 2016).

Unfortunately, the isostatic anomalies do not reveal the full effect of the upper crust heterogeneity. These structures are also isostatically compensated (locally or regionally); therefore, the gravity effect is substantially reduced by the opposing effect of the compensating masses, especially for wide sedimentary basins (Cordell et al. 1991). To refine the gravity field induced by the upper crust heterogeneity, a decompensative correction has been suggested by Zorin et al. (1985) and Cordell et al. (1991), which should be applied to the isostatic anomalies. The decompensative gravity anomalies were then employed for study of the density structure of the upper crust in the New Madrid seismic zone and Missouri gravity low (Hildenbrand et al. 1996), the Rio Grande rift (Cordell et al. 1991; Wilson et al. 2005) and sedimentary basins in South Siberia and Mongolia (e.g. Zorin et al. 1993). Recently, the decompensative gravity anomalies were calculated to study the structure of the upper crust of the Arabian plate and surroundings (Kaban et al. 2017). As was demonstrated in the last paper, the decompensative anomalies are very sensitive to the actual isostatic model and especially to the effective elastic thickness (T_e) of the lithosphere. Variations of T_e have been

recently determined for the whole Antarctic continent using the new high resolution data on bedrock topography, ice thickness and on the gravity field based on recent satellite missions and available terrestrial observations (Chen et al. 2018). Furthermore, new Moho models, which are also required for accurate determination of the isostatic and decompensative corrections, have appeared in the last years (An et al. 2015; Baranov et al. 2018; Haeger et al. 2019). These results provide a solid basis for computation of the isostatic and decompensative anomalies for Antarctica.

In the present study, we calculate the decompensative gravity anomalies for the whole Antarctic continent and use them to investigate the structure of the upper crust and particularly for determination of the sediments thickness in the basins, which are still hidden under the ice shield.

2. Tectonic Settings of Antarctica and Initial Data

2.1. Tectonic Settings

Antarctica can be divided in two tectonically very different regions: East Antarctica (EANT) is of mostly Precambrian cratonic origin with a thick and cold lithosphere, while West Antarctica (WANT) consists of several crustal micro-blocs that only reached its present day shape in the Cenozoic and is characterized by notably thinner and hotter lithosphere (Danesi and Morelli 2001; Haeger et al. 2019). The two regions are divided by the Transantarctic Mountains, a 3500 km long and 200 km wide mountain chain with elevations of up to 4500 m (Fretwell et al. 2013). While they were not uplifted by subduction or contraction (Morelli and Danesi 2004; ten Brink and Stern 1992), the exact uplift mechanism is still debated (e.g., Behrendt 1999; ten Brink and Stern 1992; van Wijk et al. 2008). EANT consists of several subglacial orogens, basins and rifts. A big plateau spans 0°–100°E and includes Dronning Maud Land, which held a key position in Gondwana formation and break-up. It includes the Archean Grunehogna craton and the juvenile Neoproterozoic remnants of the Mozambique Ocean called the Tonian Oceanic Arc Super Terrane (Jacobs et al. 2015). The plateau is interrupted by the Lambert Graben, a Mesozoic failed rift system (Lisker et al. 2003) filled by a glacier that is suggested to hold large amounts of sediments (Baranov et al. 2018). With elevations of over 1 km below sea level, the Wilkes Subglacial Basin is one of the most notable basin structures in EANT. In comparison, most of WANT exhibits bedrock topography below sea level, with the most important feature being the West Antarctic Rift System, a 750–1000 km long, mostly aseismic rift system (O'Donnell and Nyblade 2014). The bedrock topography with superimposed names of tectonic key regions is displayed in Fig. 1a.

2.2. Initial Data

In order to obtain the free air gravity field, we combine the EIGEN-6C4 model (Förste et al. 2014), containing terrestrial and satellite data from GRACE, GOCE, and LAGEOS with the purely terrestrial AntGG model (Scheinert et al. 2016). The maximum resolution for EIGEN-6C4 is 2190 spherical harmonics degree and order, but actual resolution varies locally depending on the ground data included in the gravity field model. For Antarctica, this limits the resolution to approximately 200 km (Chen et al. 2018). The AntGG model is a compilation of 13 million data points from ground-based, shipborne, and airborne gravity surveys covering 73% of Antarctica at a resolution of 10 km. Therefore, each model provides reliable data at different wavelengths: we employ the Eigen-6C4 model for $\lambda > 250$ km, since it lacks high resolution information but provides continent-wide coverage on long wavelengths and the AntGG model for $\lambda < 150$ km, since it offers high resolution information with large gaps in coverage distorting long wavelength signals (Chen et al. 2018; Haeger et al. 2019). A gradual transition is employed for 150 km $< \lambda <$ 250 km.

Subsequently, we calculate the Bouguer gravity field displayed in Fig. 2a by removing the effect of topography and of the ice and water columns. The gravity effect of each load was calculated according to (Kaban et al. 2016) using the reference densities $\rho_w = 1.03$ g/cm^3 for water, $\rho_t = 2.67$ g/cm^3 for the topography and a constant ice density of $\rho_i = 0.92$ g/cm^3 (Chen et al. 2018) within a 2°

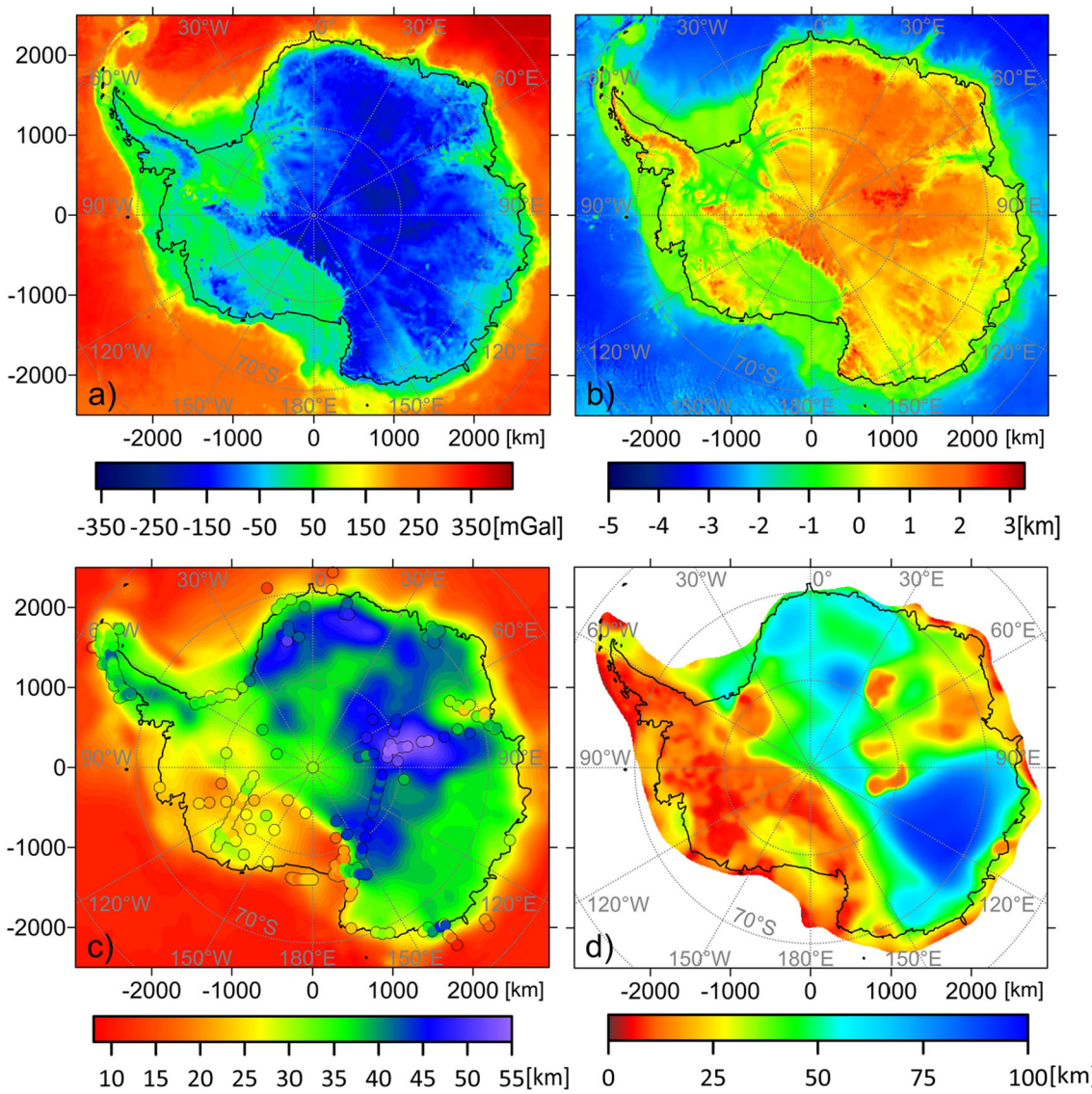

Figure 2

a Full Bouguer gravity anomalies and **b** adjusted topography calculated with respect to the reference density for the uppermost crust of 2.67 g/cm^3. **c** Map of the Moho depth with superimposed determinations from refraction, reflection, and receiver function data (circles) (An et al. 2015; Janik et al. 2014; Lamarque et al. 2015). **d** Variations of T_e obtained using the coherence method with a central wavenumber of the Morlet wavelet of 3.773 (Chen et al. 2018)

(222.4 km) radius around each grid point. We further calculate the adjusted topography t_{adj} displayed in Fig. 2b by compressing the ice and water columns to ρ_t:

$$t_{adj} = t_b + \frac{\rho_w}{\rho_t} t_w + \frac{\rho_i}{\rho_t} t_i, \qquad (1)$$

where t_b is the bedrock topography and t_w and t_i are the thickness of the water and ice column, respectively. The extent of each load was determined using surface elevation, ice thickness and bedrock topography south of 60°S from Bedmap2 (Fretwell et al. 2013) and bathymetry from RTopo-2 (Schaffer and Timmermann 2016) north of 60°S. Initial resolution of the Bedmap2 grids varies with location between 1 and 5 km, which was adjusted to a constant 10 km grid spacing in the calculations.

The calculation of the decompensative gravity anomaly requires information on the Moho depth (Fig. 2c) and effective elastic thickness variation T_e (Fig. 2d). We use the map of Moho depth variation by Haeger et al. (2019). They interpolate Moho depths from receiver function, reflection and refraction measurements within a 150 km radius and fill the remaining gaps using Moho depth constraints from surface wave tomography. The T_e variations used in this study (Chen et al. 2018) were calculated based on the coherence of Bouguer gravity and topography adjusted for variations of bedrock topography and ice thickness using cross-spectral analysis methods employing the fan wavelet technique (Kirby and Swain 2004, 2011).

3. Decompensative Gravity Anomalies

3.1. Isostatic Gravity Anomalies

In the first stage, the isostatic gravity anomalies have been determined for Antarctica and surrounding areas. In the spectral domain, the isostatic correction can be formulated as the following (Kaban et al. 2016):

$$\begin{aligned}\Delta g_{ic}(k_x,k_y) &= G_{is}(k_x,k_y)\cdot t_{adj}(k_x,k_y)\\ &= -2\pi G\rho C\cdot\exp(-k\cdot M)\cdot t_{adj}(k_x,k_y),\end{aligned} \tag{2}$$

where $k=\sqrt{k_x^2+k_y^2}$ is the wavenumber, $k_x=2\pi/\lambda_x$ and $k_y=2\pi/\lambda_y$, G is the gravitational constant, M is the Moho depth, which is chiefly associated with the isostatic compensation depth, t_{adj} is the adjusted topography and ρ is its density. The factor C characterizes the amount of the isostatic compensation depending on the wavelength and effective elastic thickness of the lithosphere (e.g. Turcotte and Schubert 1982):

$$C = \Delta\rho g/(k^4D+\Delta\rho g), \tag{3}$$

where $D=ET_e^3/[12(1-\nu^2)]$ is the flexural rigidity of the lithosphere, T_e is the effective elastic thickness of the lithosphere, E is the Young modulus, ν is the Poisson ratio, $\Delta\rho$ is the average difference of the density of topography and the upper mantle material, and g is the gravitational acceleration.

Eq. 2 cannot be used directly for calculation of the isostatic correction in the spectral domain in case of variable T_e. Therefore, a convolution of the adjusted topography with specific Green's functions depending on M and T_e is employed as suggested by Braitenberg et al. (2002), Wienecke and Braitenberg (2007) and Dill et al. (2015) for modelling of the lithosphere deformations under external load. It has been demonstrated in the above papers that this method is sufficiently accurate to describe a response of the elastic lithosphere to the external load. The isostatic correction and isostatic anomalies (Δg_i) are calculated as follows:

$$\begin{aligned}\Delta g_i(x_0,y_0) &= \Delta g_b(x_0,y_0)\\ &\quad+\iint_{-1250km}^{1250km} t_{adj}(x_0+x,y_0+y)\cdot G_{is}(x,y)\,dxdy\\ G_{is}(x,y) &= F^{-1}\left(G_{is}(k_x,k_y)\right),\end{aligned} \tag{4}$$

where F^{-1} is the inverse Fourier transform, G_{is} is the Green's function, which depends on M and T_e, $\Delta g_b(x,y)$ are the Bouguer gravity anomalies.

These anomalies still reflect the effect of the glacial isostatic adjustment and of the dynamic topography associated with the mantle convection. It has been demonstrated that this effect is dominated at the long-wavelengths chiefly exceeding 3000 km (Kaban et al. 1999, 2004). At the same time, the effect of the upper crust density variations in the isostatic anomalies anomalies is limited to the wavelengths 1000–1500 km, which are determined by the maximum value of T_e ($\sim$ 70 km, e.g. Audet and Bürgmann 2011; Tesauro et al. 2012). Therefore, to reduce the effect of mantle dynamics and GIA, we have applied a Gauss type filter on the sphere with the boundary wavelength (0.5 amplitude) equal to 2500 km (Kaban et al. 1999). To avoid the "edge" effects, the isostatic anomalies for Antarctica have been embedded in the global model of Kaban et al. (2004).

The isostatic anomalies of the gravity field (Fig. 3a) are dominated by small-scale structures. Along the Transantarctic Mountains, a dipole-like structure is visible with positive values along the western flank and negative values toward the east. The most notable negative features are located in

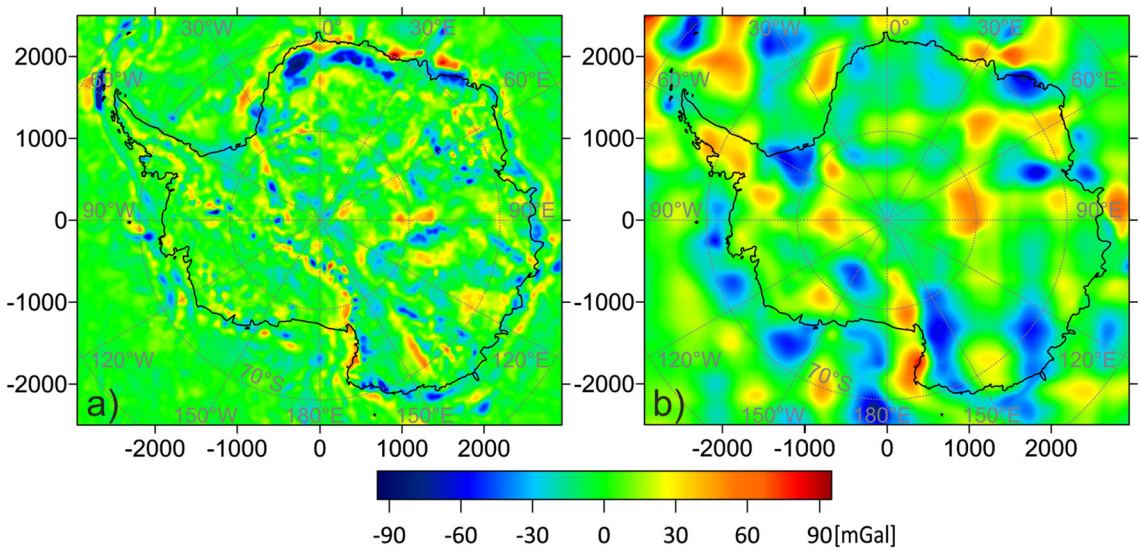

Figure 3
a Isostatic anomalies of the gravity field and **b** decompensative gravity corrections

northern Dronning Maud Land with up to − 90 mGal. A ring of positive gravity anomalies is located around the coast of EANT and is likely related to the transition from continental to oceanic lithosphere that is not sufficiently resolved in the crustal input model.

3.2. *Decompensative Anomalies of the Gravity Field*

Following Kaban et al. (2017), the decompensative correction (Δg_{dc}) can be formulated in the spectral domain as the following:

$$\Delta g_{dc}(k_x, k_y) = \frac{1}{\exp(k \cdot M)/C - 1} \cdot \Delta g_i(k_x, k_y), \quad (5)$$

where Δg_i stands for the isostatic anomalies and other terms remain as in Eq. 2. This equation is based on formulations of Zorin et al. (1985) and Cordell et al. (1991), which are extended for the case of elastic support (Kaban et al. 2017). It is clear from this equation that the decompensative correction exponentially increases with increasing wavelength and approaches infinity. It has been suggested to apply a high-pass filter to reduce the correction above some boundary wavelength (λ_0) (Cordell et al. 1991). The long-wavelength component is already excluded from the isostatic anomalies in Fig. 3a, however, the decompensative correction can still be overestimated as demonstrated in Kaban et al. (2017). Following their argumentation, a high-pass filter starting from the wavelength 1500 km with a gradual decrease toward longer wavelengths has been applied to Eq. 5.

The decompensative correction is calculated using the same Green's functions technique as for the isostatic anomalies (Eq. 4) and is displayed in Fig. 3b and exhibits larger scale features compared to the isostatic anomalies. The most notable negative decompensative corrections are located in Enderby Land (− 75 mGal), in the Lambert Graben (− 64 mGal), the Filchner-Ronne Ice Shelf (− 60 mGal), and the West Antarctic Rift System (− 50 mGal). A similar dipole structure as in the isostatic anomalies is visible along the Transantarctic Mountains and in the Wilkes Subglacial Basin with positive values of up to 80 mGal in the west and negative values of up to − 62 mGal in the east. Positive corrections are also located in the Antarctic Peninsular and around the Lambert Graben minimum (up to 47 and 52 mGal, respectively).

The final decompensative gravity anomalies are calculated through:

$$\Delta g_d = \Delta g_i + \Delta g_{dc}, \quad (6)$$

and are shown in Fig. 4. The main negative anomalies can be found in northern Dronning Maud Land (− 120 mGal), in Enderby Land (− 143 mGal), in

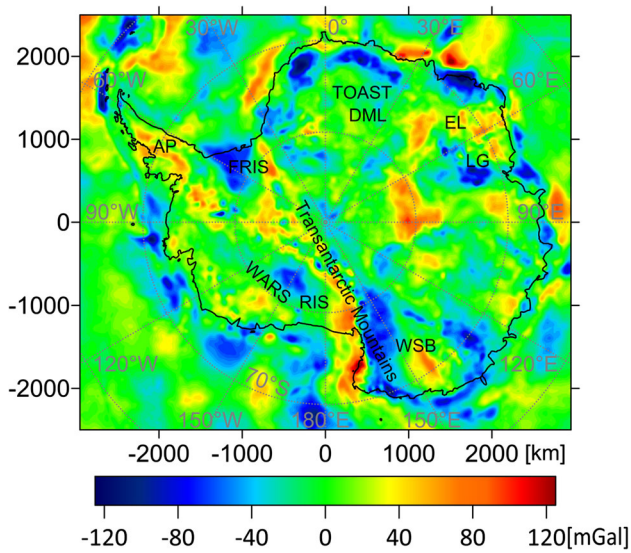

Figure 4
Decompensative gravity anomalies

the Lambert Graben (− 110 mGal), the Filchner-Ronne Ice Shelf (− 80 mGal) and the West Antarctic Rift System (− 73 mGal). Another negative anomaly (− 110 mGal), interrupted by a narrow, elongated, positive anomaly in the Northern Basin (80 mGal), exists around the Wilkes Subglacial Basin and forms a dipole-like structure along the Transantarctic Mountains with the western flank exhibiting positive decompensative anomalies (138 mGal). This positive feature continues along the Transantarctic Mountains toward the Antarctic Peninsula. The Lambert Graben exhibits strong negative anomalies of up to − 110 mGal while the surrounding region is characterized by positive values of up to 104 mGal.

4. Discussion

The decompensative gravity anomalies can help us understand the structure of the uppermost crust of Antarctica where direct measurements are still rare. An important if not the most important factor causing negative anomalies is the presence of sediments. Since knowledge about their distribution over Antarctica is still limited, no correction involving sediment has been applied in the initial processing. We calculate the thickness of sediments by assuming that negative decompensative anomalies are purely caused by sediments. This assumption is not valid all over the study area, therefore our results might be overestimated in some places. As well, some basins may be characterized by high density; in this case, the actual thickness could be higher than predicted. As density within sedimentary basins increases with depth in different ways for different basins and tectonic background, it would be ideal, if density–depth relations for each individual basin were used. However, these data don't exist for Antarctica and therefore standard density–depth curves for continental and oceanic basins (Mooney and Kaban 2010) are used in the calculations. The resulting uncertainties in sediment thickness estimates depend strongly on the thickness of the sedimentary basin. Assuming that the uncertainties associated with average density variations within a basin reach up to $\pm$ 0.05 g/cm^3 and a decompensative gravity anomaly of − 40 mGal, the density uncertainties translate into thickness uncertainties of up to $\pm$ 1 km. It should also be noted, that not every sedimentary basins may be detectible using this approach. As mentioned above, old cratonic sediment basins can be characterized by very dense sediments that are almost indistinguishable from the crystalline crust using gravity data, which has been shown for e.g. the

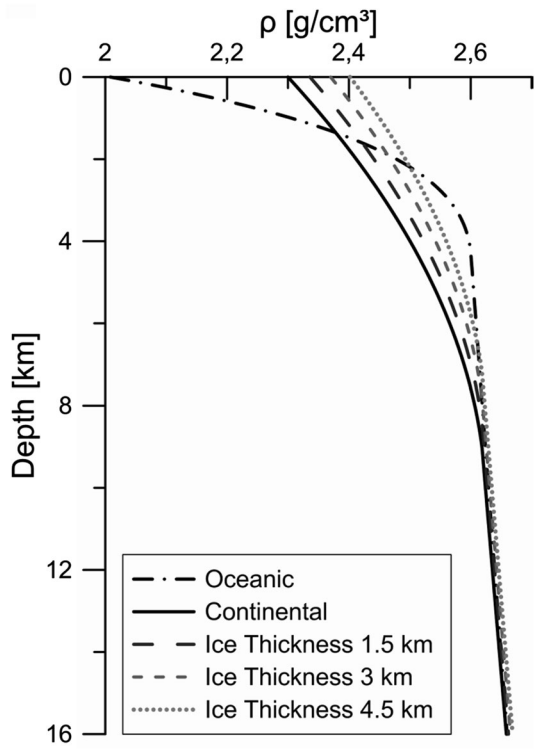

Figure 5
Variation of sediment density with depth for oceanic and continental settings (Mooney and Kaban 2010) with the compacting effect of grounded ice loads of 0, 1.5, 3 and 4.5 km thickness

Illinois and the Michigan Basin (Mooney and Kaban 2010). Additional compaction might be caused by the ice load over the majority of the Antarctic continent. Potential influence of this effect on the estimated thickness has been investigated by shifting the original density–depth curves. Where the ice is grounded, the ice thickness was converted into equivalent sediment thickness with respect to the average density of the first 1.5 km of sediments ($\rho_{eq} = 2.34$ g/cm^3) and the density–depth curves were shifted accordingly. The density–depth curves for the oceanic domain and for the continental one with the compacting effect of the ice load for 0, 1.5, 3 and 4.5 km are plotted in Fig. 5.

The decompensative anomalies (Fig. 4) do not contain the long-wavelength component and their average is equal to zero. However, the actual effect of the upper crust relative to a standard reference density of 2.7 g/cm^3 should be negative (e.g. Mooney and Kaban 2010; Kaban et al. 2014). Density variations in the crystalline crust relative to this value are close to zero on the average (Christensen and Mooney 1995), while density of sediments is generally lower. Therefore, for estimation of the sediment thickness we should shift downward the field in Fig. 4 by some constant level. It is hardly possible to determine it from the existing data, however, estimates for other continents demonstrate that the average gravity effect of the upper crust is quite stable. It is equal to − 17.5 mGal for North America (Kaban et al. 2014) and − 14.6 mGal for Australia (Tesauro et al. 2018), for which continents very detailed models of the sedimentary cover are available. For Antarctica we use the lowest value assuming that sedimentation is partially restricted due to glaciation and sediments might be more compressed under the additional ice load. This value is anyway arbitrary and possible uncertainty might reach ± 3–4 mGal translating into uncertainties in sediment thickness of up to ± 0.9 km for sediment basins of 5 km depth. For the deeper sedimentary basins this uncertainty increases, but the effect of the density uncertainty is much larger anyway. This is taken into account in the interpretation of the results.

The resulting sediment thickness estimates straight from the decompensative gravity anomaly and considering the − 14.6 mGal shift, both with and without considering compaction caused by the ice shield are shown in Fig. 6. The maximum sediment thickness is limited to 16 km, because the density of deeper sediments would be indistinguishable from crystalline rocks. Adding the corrections for the ice load and for the reduced gravity effect of the upper crust in the presence of sediments only changes the amplitude, not the distribution of sediment deposits, with both effects increasing the thickness. Despite the uncertainty in the upper crustal correction, we will discuss the sediment thicknesses obtained including both corrections from this point forward. Therefore, and because calculations of the actual thickness strongly depend on the chosen density–depth relationship which is still unknown for Antarctic sediment basins, we emphasize that all discussions of the results should be done qualitatively instead of quantitatively.

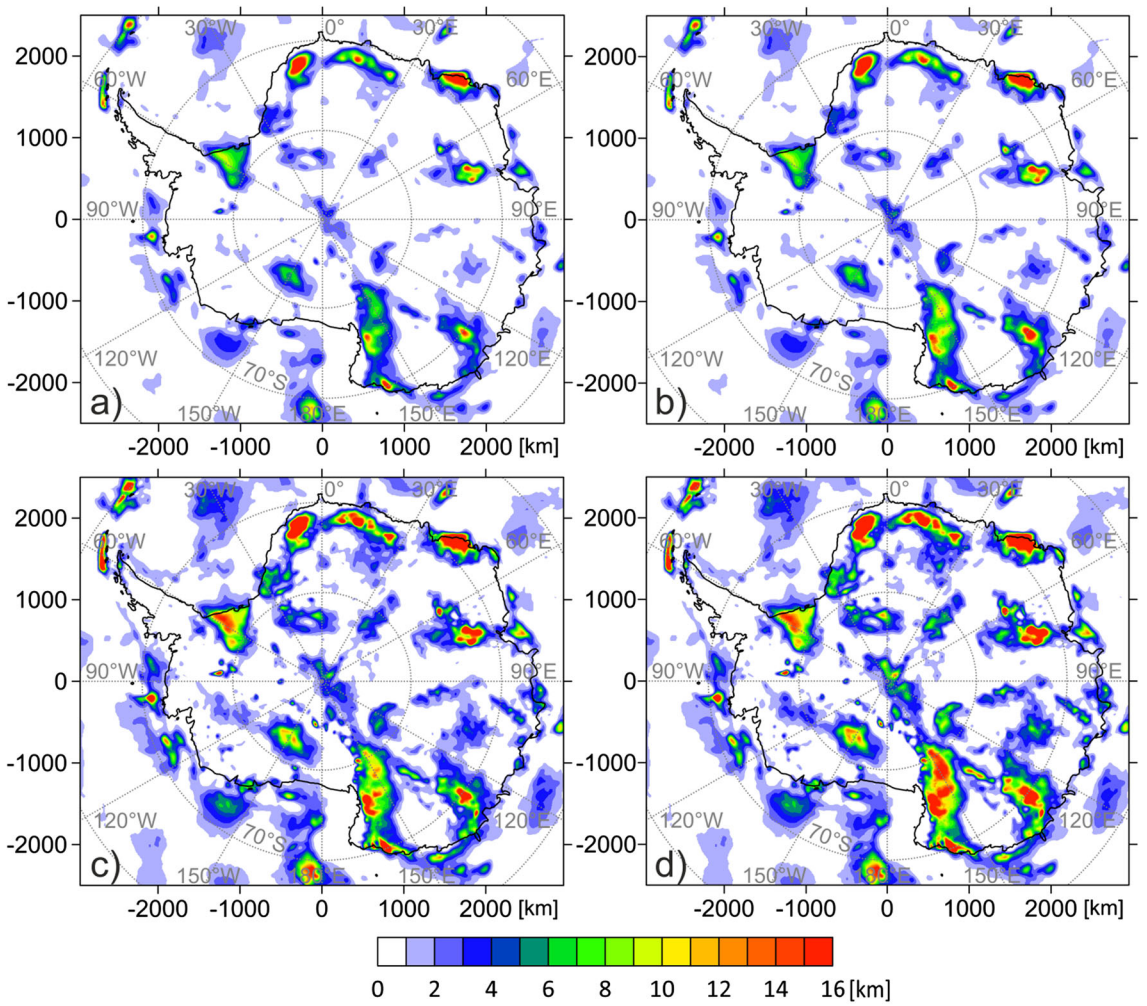

Figure 6
Sediment thickness calculated from the decompensative gravity anomalies (top row). A correction of the upper crust for the decompensative gravity anomalies of − 14.6 mGal is considered in the bottom row. Left column: sediment thickness calculations without ice load. Right column: sediment thickness considering compaction caused by ice loads

The most notable feature is the dipole like structure around the Transantarctic Mountains. The western flank is characterized by high decompensative anomalies while the eastern region as well as the western margin of the adjacent Wilkes Subglacial Basin exhibit very low values. This could be caused by local isostatic disturbances originated from extension forces of prior rifting in the West Antarctic Rift System or from dynamic uplift of the Transantarctic Mountains of possibly thermal origin as suggested by several previous studies (e.g., Behrendt 1999; Smith and Drewry 1984; ten Brink and Stern 1992). Lawrence et al. (2006) state that uplift of the Transantarctic Mountains can be explained by conductive heating between cold EANT and warm WANT alone along the entire mountain chain also explaining the positive decompensative anomaly values along the continuation of the Transantarctic Mountains. They also state, that this uplift was asymmetrical causing erosion of younger sediments on the coastward side, exposing denser basement rock and older sediments. This together with the large sediment dispositions in the southern Wilkes Subglacial Basin suggested by Frederick et al. (2016) can also cause the negative decompensative anomalies we observe. However, even though we confirm the

presence of large sediment deposits, attributing these negative variations purely to sediments as done in our calculations leading to thicknesses of up to 16 km likely represents an overestimation of the sediment thickness. This value can be reduced if the sediments have lower density than suggested. The western Wilkes Subglacial Basin exhibits low sedimentation (Frederick et al. 2016) and high decompensative anomaly values which is likely related to denser basement rocks. Adjacent, further sediment infill is detected. The border of this feature coincides with the Adventure Trench that has been shown to have $\sim$ 10 km sediment infill (Ferraccioli et al. 2001), but is not limited to the trench.

Negative decompensative gravity anomalies suggesting the presence of significant sediment accumulations are also found in the West Antarctic Rift System with a maximum infill at the transition to the Ross Ice Shelf and a continuation in the western Ross Sea. Sediment infill of the Rift System has been documented by several studies in the past (e.g., Baranov et al. 2018; Laske et al. 2013), supporting our interpretation. Anandakrishnan et al. (1998) estimated a sediment layer of 2.8 km under an ice stream (roughly 82°S, 121°E) agreeing well with our estimates of $\sim$ 2.5 km. While the above mentioned studies mapped a relatively constant sediment infill of 2–3 km along most of the West Antarctic Rift System, the newly found thick sediment cover at the ice shelf transition offers new insight into variation in sediment thickness along the Rift System. Wobbe et al. (2014) found evidence of a thick sediment layer of up to 8 km under most of the Ross Ice Shelf. This sediment layer continues in the Ross Sea with major infill in the Victoria Land Basin, the Central Trough and the Eastern Basin (Behrendt et al. 1991; Trey et al. 1999). We only map sediment infill in the western Ross Ice Shelf and in the Eastern Basin, with the positive decompensative anomaly attributed to Transantarctic Mountain uplift described above masking potential sediments in the eastern ice shelf region and in the other two sediment basins in the Ross Sea. Trey et al. (1999) also predict high density upper crust below the sediment basins, further equalizing the gravity effect of low density sediments. Lindeque et al. (2016) further determined sediment thicknesses along a seismic profile in the Amundsen Sea Basin and found maximum thicknesses of almost 4 km around 145°W, corresponding well with the location of a maximum in sediment infill in our determinations.

The other large Antarctic ice shelf, the Filchner-Ronne Ice Shelf is also characterized by low decompensative gravity anomalies that translate into sediment thicknesses of over 15 km. Two seismic profiles crossing the Filchner-Ronne Ice shelf were conducted in the past (Hübscher et al. 1996; Leitchenkov and Kudryavtzev 1997), independently determining sediment layers of up to 13 and 15 km, respectively, agreeing well with our determinations. High sediment infill is expected in the Lambert Graben when converting the low compensative gravity anomalies to sediment deposits, which is confirmed by previous studies (Harrowfield et al. 2005; Holdgate et al. 2005). However, thickness determinations only exist offshore in the Prydz Bay (Stagg et al. 2004). Their sediment thickness determinations of 5–8 km lie well below our estimates of up to 13 km, suggesting an overestimation in both the Prydz Bay and the Lambert Graben. A ring of high decompensative gravity anomalies surrounds the Lambert Graben, possibly caused by older, denser upper crustal rocks. Furthermore, Chen et al. (2018) predict notable lithospheric weakening in the graben structure compared to higher effective elastic thickness estimates in the surroundings. This transition from local to regional compensation might cause disturbances of the isostatic equilibrium insufficiently corrected for in the initial calculations, reflecting in the above described anomaly structures.

Dronning Maud Land is chiefly governed by negative decompensative gravity anomalies that can be explained by sediment deposits. The largest sediment accumulations are predicted in coastal Dronning Maud Land in the vicinity of the Grunehogna craton and the Tonian Oceanic Arc Super Terrane and in northern Enderby Land. The coverage of studies analyzing sediments in this region is still sparse, making direct comparison difficult. Curtis and Riley (2003) and Krynauw et al. (1994) found evidence of sediment deposits when investigating the Grunehogna nunataks, however no geophysical estimate of sediment thickness or density has been conducted. Gupta et al. (2017) studied the subsurface

below Maitri station (70.76°S, 11.73°E) at the northern edge of the decompensative anomaly minimum estimating a sediment layer of 1.5 km. This supports our interpretation of the feature as a sediment basin of possibly marine origin, as the Tonian Oceanic Arc Super Terrane is proposed to be a remnant of the Mozambique Ocean (Jacobs et al. 2015). Further south, we find thinner sediment deposits underlying parts of the Recovery Glacier and the Bailey Ice Stream. In the vicinity, Bamber et al. (2006) detected sediment deposits of $\sim$ 3 km underlying the Slessor Tributary North using aeromagnetic measurements.

5. Conclusions

Here, we present a continent wide study of the decompensative gravity anomaly over Antarctica revealing upper crustal structures. Isostatic gravity anomalies are widely used for this purpose; they are however still reduced by deep compensating masses. The decompensative correction over Antarctica reaches values of up to $\pm$ 70 mGal. Hence, neglecting this effect might lead to misinterpretation of upper crustal structures. Large positive decompensative gravity anomalies are located around a minimum in the Lambert Graben, which are probably caused by higher density, old crystalline crust combined with isostatic disturbances induced by the transition from regional to local compensation as suggested by analyzing effective elastic thickness variations in this region (Chen et al. 2018).

Negative anomalies are translated into sediment thickness, which is still largely unknown for Antarctica due to the thick ice shield covering the majority of the continent, taking into account the compacting effect of these ice loads on sediment density. The resulting sediment thicknesses are subject to large uncertainties caused by unknown density–depth relationships for the individual basins and the unknown reducing gravity effect of the upper crust. Therefore, they should be understood as qualitative instead of quantitative estimates.

We confirm the presence of major sediment basins in the Filchner-Ronne Ice Shelf, the northern Wilkes Subglacial Basin and the Lambert Graben. Further sedimentary deposits that were previously not or only partially mapped are detected in both EANT and WANT. Thus, we find maximum sediment infill of the West Antarctic Rift System at the transition from the continent to the Ross Ice Shelf and thick sediment basins along the coast of Dronning Maud Land and Enderby Land. Additionally, sediments are found underlying major ice streams of the East Antarctic Ice Shield like the Recovery Glacier, which might have played an important role in ice stream formation and dynamics. Known sedimentary deposits such as in the Ross Sea are not mapped in this study but were masked by positive decompensative gravity anomalies caused by local isostatic disturbances due to the dynamic (possibly thermally driven, Lawrence et al. 2006), uplift of the Transantarctic Mountains.

Acknowledgements

We thank three anonymous reviewers and the editor Carla Braitenberg for their valuable comments that have greatly improved the manuscript. This study was supported by DFG (German Research Foundation), SPP-1788 Dynamic Earth (Grants KA2669/4-1 and KA2669/4-2). The results of this study are available in digital form from the authors upon request.

References

Aitken, A. R. A., Young, D. A., Ferraccioli, F., Betts, P. G., Greenbaum, J. S., Richter, T. G., et al. (2014). The subglacial geology of Wilkes Land, East Antarctica. *Geophysical Research Letters, 41*(7), 2390–2400. https://doi.org/10.1002/2014GL059405.

An, M., Wiens, D. A., Zhao, Y., Feng, M., Nyblade, A. A., Kanao, M., et al. (2015). S-velocity model and inferred Moho topography beneath the Antarctic Plate from Rayleigh waves. *Journal of Geophysical Research: Solid Earth, 120*(1), 359–383. https://doi.org/10.1002/2014JB011332.

Anandakrishnan, S., Blankenship, D. D., Alley, R. B., & Stoffa, P. L. (1998). Influence of subglacial geology on the position of a West antarctic ice stream from seismic observations. *Nature, 394*(6688), 62–65. https://doi.org/10.1038/27889.

Audet, P., & Bürgmann, R. (2011). Dominant role of tectonic inheritance in supercontinent cycles. *Nature Geosciences, 4,* 184–187. https://doi.org/10.1038/ngeo1080.

Bamber, J. L., Ferraccioli, F., Joughin, I., Shepherd, T., Rippin, D. M., Siegert, M. J., et al. (2006). East Antartic ice stream tributary underlain by major sedimentary basin. *Geology, 34*(1), 33–36. https://doi.org/10.1130/G22160.1.

Baranov, A., Tenzer, R., & Bagherbandi, M. (2018). *Combined gravimetric–seismic crustal model for Antarctica Surveys in Geophysics* (Vol. 39). The Netherlands: Springer. https://doi.org/10.1007/s10712-017-9423-5.

Behrendt, J. C. (1999). Crustal and lithospheric structure of the west Antarctic Rift System from geophysical investigations—A review. *Global and Planetary Change, 23*(1–4), 25–44. https://doi.org/10.1016/S0921-8181(99)00049-1.

Behrendt, J. C., LeMasurier, W. E., Cooper, A. K., Tessensohn, F., Tréhu, A., & Damaske, D. (1991). Geophysical studies of the West Antarctic Rift System. *Tectonics, 10*(6), 1257–1273. https://doi.org/10.1029/91TC00868.

Bell, R. E., Blankenship, D. D., Finn, C. A., Morse, D. L., Scambos, T. A., Brozena, J. M., et al. (1998). Influence of subglacial geology on the onset of a West Antarctic ice stream from aerogeophysical observations. *Nature, 394*(6688), 58–62.

Blakely, R. J. (1995). *Potential Theory in Gravity and Magnetic Applications*. London: Cambridge University Press.

Braitenberg, C., Ebbing, J., & Götze, H. J. (2002). Inverse modelling of elastic thickness by convolution method—The eastern Alps as a case example. *Earth and Planetary Science Letters, 202*(2), 387–404. https://doi.org/10.1016/S0012-821X(02)00793-8.

Chen, B., Haeger, C., Kaban, M. K., & Petrunin, A. G. (2018). Variations of the effective elastic thickness reveal tectonic fragmentation of the Antarctic lithosphere. *Tectonophysics, 1,* 746. https://doi.org/10.1016/j.tecto.2017.06.012.

Christensen, N. I., & Mooney, W. D. (1995). Seismic velocity structure and composition of the continental crust: A global review. *Journal of Geophysical Research, 100,* 9761–9788.

Cordell, L., Zorin, Y. A., & Keller, G. R. (1991). The decompensative gravity anomaly and deep structure of the region of the Rio Grande rift (1978–2012). *Journal of Geophysical Research Solid Earth, 96*(B4), 6557–6568.

Curtis, M. L., & Riley, T. R. (2003). Mobilization of fluidized sediment during sill emplacement, western Dronning Maud Land, East Antarctica. *Antarctic Science, 15*(3), 393–398. https://doi.org/10.1017/S0954102003001408.

Danesi, S., & Morelli, A. (2001). Structure of the upper mantle under the Antarctic Plate from surface wave tomography. *Geophysical Research Letters, 28*(23), 4395–4398. https://doi.org/10.1029/2001GL013431.

Dill, R., Klemann, V., Martinec, Z., & Tesauro, M. (2015). Applying local Green's functions to study the influence of the crustal structure on hydrological loading displacements. *Journal of Geodynamics, 88,* 14–22.

Ebbing, J., Braitenberg, C., & Wienecke, S. (2007). Insights into the lithospheric structure and the tectonic setting of the Barents Sea region from isostatic considerations. *Geophysical Journal International, 171,* 1390–1403. https://doi.org/10.1111/j.1365-246x.2007.03602.x.

Ferraccioli, F., Coren, F., Bozzo, E., Zanolla, C., Gandolfi, S., Tabacco, I., et al. (2001). Rifted(?) crust at the East Antarctic Craton margin: gravity and magnetic interpretation along a traverse across the Wilkes Subglacial Basin region. *Earth and Planetary Science Letters, 192*(3), 407–421. https://doi.org/10.1016/S0012-821X(01)00459-9.

Förste, C., Bruinsma, S., Abrikosov, O., Flechtner, F., Marty, J.-C., Lemoine, J.-M., et al. (2014). EIGEN-6C4—The latest combined global gravity field model including GOCE data up to degree and order 1949 of GFZ Potsdam and GRGS Toulouse. *EGU General Assembly, 16,* 3707. https://doi.org/10.5880/icgem.2015.1.

Frederick, B. C., Young, D. A., Blankenship, D. D., Richter, T. G., Kempf, S. D., Ferraccioli, F., et al. (2016). Distribution of subglacial sediments across the Wilkes Subglacial Basin, East Antarctica. *Journal of Geophysical Research F: Earth Surface, 121*(4), 790–813. https://doi.org/10.1002/2015JF003760.

Fretwell, P., Pritchard, H. D., Vaughan, D. G., Bamber, J. L., Barrand, N. E., Bell, R., et al. (2013). Bedmap 2: improved ice bed, surface and thickness datasets for Antarctica. *Cryosphere, 7*(1), 375–393. https://doi.org/10.5194/tc-7-375-2013.

Gupta, S., Kanna, N., & Akilan, A. (2017). Volcanic passive continental margin beneath Maitri station in central DML, East Antarctica: Constraints from crustal shear velocity through receiver function modelling. *Polar Research, 36,* 1. https://doi.org/10.1080/17518369.2017.1332947.

Haeger, C., Kaban, M. K., Tesauro, M., Petrunin, A. G., & Mooney, W. D. (2019). 3D density, thermal and compositional model of the Antarctic lithosphere and implications for its evolution. *Geochemistry, Geophysics, Geosystems, 2005,* 1–20. https://doi.org/10.1029/2018GC008033.

Harrowfield, M., Holdgate, G. R., Wilson, C. J. L., & McLoughlin, S. (2005). Tectonic significance of the Lambert graben, East Antarctica: reconstructing the Gondwanan rift. *Geology, 33*(3), 197–200. https://doi.org/10.1130/G21081.1.

Hildenbrand, T. G., Griscom, A., Van Schmus, W. R., & Stuart, W. D. (1996). Quantitative investigations of the Missouri gravity low: A possible expression of a large, Late Precambrian batholith intersecting the New Madrid seismic zone (1978–2012). *Journal of Geophysical Research Solid Earth, 101*(B10), 21921–21942.

Holdgate, G. R., McLoughlin, S., Drinnan, A. N., Finkelman, R. B., Willett, J. C., & Chiehowsky, L. A. (2005). Inorganic chemistry, petrography and palaeobotany of Permian coals in the Prince Charles Mountains, East Antarctica. *International Journal of Coal Geology, 63*(1–2 SPEC. ISS.), 156–177. https://doi.org/10.1016/j.coal.2005.02.011.

Hübscher, C., Jokat, W., & Miller, H. (1996). Structure and origin of southern Weddell Sea crust: results and implications. *Geological Society, London, Special Publications, 108*(1), 201–211. https://doi.org/10.1144/GSL.SP.1996.108.01.15.

Jachens, R.C., & Moring, C. (1990). Maps of the thickness of Cenozoic deposits and the isostatic residual gravity over basement for Nevada. *U.S. Geological Survey Open File Report*, 90-404.

Jacobs, J., Elburg, M., Läufer, A., Kleinhanns, I. C., Henjes-Kunst, F., Estrada, S., et al. (2015). Two distinct Late Mesoproterozoic/Early Neoproterozoic basement provinces in central/eastern Dronning Maud Land, East Antarctica: the missing link, 15–21°E. *Precambrian Research, 265,* 249–272. https://doi.org/10.1016/j.precamres.2015.05.003.

Janik, T., Grad, M., Guterch, A., & Środa, P. (2014). The deep seismic structure of the Earth's crust along the Antarctic Peninsula-A summary of the results from Polish geodynamical expeditions. *Global and Planetary Change, 123,* 213–222. https://doi.org/10.1016/j.gloplacha.2014.08.018.

Kaban, M. K., El Khrepy, S., & Al-Arifi, N. (2016). Isostatic model and isostatic gravity anomalies of the Arabian plate and surroundings. *Pure and Applied Geophysics, 173*(4), 1211–1221. https://doi.org/10.1007/s00024-015-1164-0.

Kaban, M. K., El Khrepy, S., & Al-Arifi, N. (2017). Importance of the decompensative correction of the gravity field for study of the upper crust: Application to the Arabian plate and surroundings. *Pure and Applied Geophysics, 174*(1), 349–358.

Kaban, M. K., Schwintzer, P., & Reigber, Ch. (2004). A new isostatic model of the lithosphere and gravity field. *Journal of Geodesy, 78,* 368–385.

Kaban, M. K., Schwintzer, P., & Tikhotsky, S. A. (1999). Global isostatic residual geoid and isostatic gravity anomalies. *Geophysical Journal International, 136,* 519–536.

Kaban, M. K., Tesauro, M., Mooney, W. D., & Cloetingh, S. A. P. L. (2014). Density, temperature, and composition of the North American lithosphere—New insights from a joint analysis of seismic, gravity, and mineral physics data: 1. Density structure of the crust and upper mantle. *Geochemistry, Geophysics, Geosystems, 3,* 15. https://doi.org/10.1002/2014gc005483.-&gt.

Kirby, J. F., & Swain, C. J. (2004). Global and local isostatic coherence from the wavelet transform. *Geophysical Research Letters, 31*(24), 1–5. https://doi.org/10.1029/2004GL021569.

Kirby, J. F., & Swain, C. J. (2011). Improving the spatial resolution of effective elastic thickness estimation with the fan wavelet transform. *Computers & Geosciences, 37*(9), 1345–1354. https://doi.org/10.1016/j.cageo.2010.10.008.

Krynauw, J. R., Behr, H. J., & Vandenkerkhof, A. M. (1994). Sill emplacement in wet sediments—Fluid inclusion and cathodoluminescence studies at grunehogna, western Dronning-Maud-Land, Antarctica. *Journal of the Geological Society, 151,* 777–794. https://doi.org/10.1144/gsjgs.151.5.0777.

Lamarque, G., Barruol, G., Fontaine, F. R., Bascou, J., & Menot, R.-P. (2015). Crustal and mantle structure beneath the Terre Adelie Craton, East Antarctica: insights from receiver function and seismic anisotropy measurements. *Geophysical Journal International, 200*(2), 807–821. https://doi.org/10.1093/gji/ggu430.

Langenheim, V.E., & Jachens, R.C. (1996). Gravity data collected along the Los Angeles regional seismic experiment (LARSE) and preliminary model of regional density variations in basement rocks, southern California. *U.S. Geological Survey Open File Report*, 96-682.

Laske, G., Masters, G., Ma, Z., Pasyanos, M. (2013). Update on CRUST1. 0—A 1-degree global model of Earth's crust. *Geophysical Research Abstracts*, *15*, 2658. Retrieved from http://meetingorganizer.copernicus.org/EGU2013/EGU2013-2658.pdf.

Lawrence, J. F., Wiens, D. A., Nyblade, A. A., Anandakrishnan, S., Shore, P. J., & Voigt, D. (2006). Crust and upper mantle structure of the transantarctic mountains and surrounding regions from receiver functions, surface waves, and gravity: Implications for uplift models. *Geochemistry, Geophysics, Geosystems*. https://doi.org/10.1029/2006GC001282.

Leitchenkov, G. L., & Kudryavtzev, G. A. (1997). Structure and Origin of the Earth's Crust in the Weddell Sea Embayment (beneath the Front of the Filchner and Ronne Ice Shelves) from Deep Seismic Sounding data. *Polarforschung, 67*(3), 143–154.

Lindeque, A., Gohl, K., Henrys, S., Wobbe, F., & Davy, B. (2016). Seismic stratigraphy along the Amundsen Sea to Ross Sea continental rise: a cross-regional record of pre-glacial to glacial processes of the West Antarctic margin. *Palaeogeography, Palaeoclimatology, Palaeoecology, 443,* 183–202. https://doi.org/10.1016/j.palaeo.2015.11.017.

Lisker, F., Brown, R., & Fabel, D. (2003). Denudational and thermal history along a transect across the Lambert Graben, northern Prince Charles Mountains, Antarctica, derived from apatite fission track thermochronology. *Tectonics, 22*(5), 1055. https://doi.org/10.1029/2002TC001477.

Mooney, W. D., & Kaban, M. K. (2010). The North American upper mantle: density, composition, and evolution. *Journal of Geophysical Research, 115,* B12424. https://doi.org/10.1029/2010jb000866.

Morelli, A., & Danesi, S. (2004). Seismological imaging of the Antarctic continental lithosphere: A review. *Global and Planetary Change, 42,* 155–165. https://doi.org/10.1016/j.gloplacha.2003.12.005.

O'Donnell, J. P., & Nyblade, A. A. (2014). Antarctica's hypsometry and crustal thickness: Implications for the origin of anomalous topography in East Antarctica. *Earth and Planetary Science Letters, 388,* 143–155. https://doi.org/10.1016/j.epsl.2013.11.051.

Schaffer, J., Timmermann, R. (2016). Greenland and Antarctic ice sheet topography, cavity geometry, and global bathymetry (RTopo-2), links to NetCDF files. *PANGAEA*. https://doi.org/10.1594/PANGAEA.856844 (Supplement to: Schaffer, J., Timmermann, R., Arndt, J. E., Kristensen, S. S., Mayer, C., Morlighem, M., Steinhage, D. (2016). A global, high-resolution data set of ice sheet topography, cavity geometry, and ocean bathymetry. *Earth System Science Data*, *8*(2), 543–557. https://doi.org/10.5194/essd-8-543-2016)

Scheinert, M., Ferraccioli, F., Schwabe, J., Bell, R., Studinger, M., Damaske, D., et al. (2016). New Antarctic gravity anomaly grid for enhanced geodetic and geophysical studies in Antarctica. *Geophysical Research Letters, 43*(2), 600–610. https://doi.org/10.1002/2015GL067439.

Simpson, R. W., Jachens, R. C., Blakely, R. J., & Saltus, R. W. (1986). A new isostatic residual gravity map of the conterminous United States with a discussion on the significance of isostatic residual anomalies. *Journal of Geophysical Research: Solid Earth, 91,* 8348–8372.

Smith, A. G., & Drewry, D. J. (1984). Delayed phase change due to hot asthenosphere causes Transantarctic uplift? *Nature, 309,* 536–538.

Smith, A. M., Jordan, T. A., Ferraccioli, F., & Bingham, R. G. (2013). Influence of subglacial conditions on ice stream dynamics: Seismic and potential field data from Pine Island Glacier, West Antarctica. *Journal of Geophysical Research: Solid Earth, 118*(4), 1471–1482. https://doi.org/10.1029/2012JB009582.

Stagg, H. M. J., Colwel, J. B., Direen, N. G., O'Brien, P. E., Bernardel, G., Borissova, I., et al. (2004). Geology of the continental margin of Enderby and Mac. Robertson Lands, East Antarctica: Insights from a regional data set. *Marine Geophysical Researches, 25*(3–4), 183–219. https://doi.org/10.1007/s11001-005-1316-1.

ten Brink, U., & Stern, T. (1992). Rift flank uplifts and Hinterland basins—Comparison of the Transantarctic Mountains with the great escarpment of Southern Africa. *Journal of Geophysical Research-Solid Earth, 97*(B1), 569–585. https://doi.org/10.1029/91JB02231.

Tesauro, M., Audet, P., Kaban, M. K., Bürgmann, R., & Cloetingh, S. (2012). The effective elastic thickness of the continental

lithosphere: Comparison between rheological and inverse approaches. *Geochemistry Geophysics Geosystems (G3), 13,* Q09001.

Tesauro, M., Kaban, M. K., Aitken, A. (2018). Temperature and compositional variation in the Australian lithospheric mantle (Geophysical Research Abstracts; vol. 20, EGU2018-7661, 2018), General Assembly European Geosciences Union.

Trey, H., Cooper, A. K., Pellis, G., Della Vedova, B., Cochrane, G., Brancolini, G., et al. (1999). Transect across the West Antarctic rift system in the Ross Sea, Antarctica. *Tectonophysics, 301*(1–2), 61–74. https://doi.org/10.1016/S0040-1951(98)00155-3.

Turcotte, D. L., & Schubert, G. (1982). *Geodynamics* (2nd ed.). Cambridge: Cambridge University Press.

van Wijk, J. W., Lawrence, J. F., & Driscoll, N. W. (2008). Formation of the Transantarctic Mountains related to extension of the West Antarctic Rift system. *Tectonophysics, 458*(1–4), 117–126. https://doi.org/10.1016/j.tecto.2008.03.009.

Wienecke, S., & Braitenberg, C. (2007). A new analytical solution estimating the flexural rigidity in the Central Andes. *Geophysical Journal International*. https://doi.org/10.1111/j.1365-246X.2007.3396.x.

Wilson, D., Aster, R., West, M., Ni, J., Grand, S., Gao, W., et al. (2005). Lithospheric structure of the Rio Grande rift. *Nature, 433*(7028), 851–855.

Wobbe, F., Lindeque, A., & Gohl, K. (2014). Anomalous South Pacific lithosphere dynamics derived from new total sediment thickness estimates off the West Antarctic margin. *Global and Planetary Change, 123,* 139–149. https://doi.org/10.1016/j.gloplacha.2014.09.006.

Zorin, Y. A., Belichenko, V. G., Turutanov, E. K., Kozhevnikov, V. M., Ruzhentsev, S. V., Dergunov, A. B., et al. (1993). The south Siberia-central Mongolia transect. *Tectonophysics, 225*(4), 361–378.

Zorin, Y. A., Pismenny, B. M., Novoselova, M. R., & Turutanov, E. K. (1985). Decompensative gravtity anomalies. *Geologia i Geofizika, 8,* 104–108.

(Received February 19, 2019, revised April 29, 2019, accepted May 2, 2019, Published online May 14, 2019)